Energy fluxes and shell-to-shell transfers in three-dimensional decaying magnetohydrodynamic turbulence

Olivier Debliquy
Statistical and Plasma Physics, Université Libre de Bruxelles, CP231, Campus Plaine, 1050 Brussels, Belgium

Mahendra K. Verma
Department of Physics, Indian Institute of Technology, Kanpur 208016, India

Daniele Carati
Statistical and Plasma Physics, Université Libre de Bruxelles, CP231, Campus Plaine, 1050 Brussels, Belgium

(Received 31 August 2004; accepted 12 January 2005; published online 30 March 2005)

A spectral analysis of the energy cascade in magnetohydrodynamics (MHD) is presented using high-resolution direct numerical simulation of decaying isotropic turbulence. The Fourier representations of both the velocity and the magnetic fields are split into subsets that correspond to shells of wave vectors. A detailed study of the shell-to-shell interactions is performed and a comparison with theoretical prediction based on field-theoretic method is proposed. Two different definitions for the forward and backward energy transfers are suggested. They provide diagnostics that can be used in order to assess subgrid-scale modeling in large eddy simulation for turbulent MHD systems. © *2005 American Institute of Physics*. [DOI: 10.1063/1.1867996]

I. INTRODUCTION

Magnetohydrodynamic (MHD) turbulence in three-dimensional systems shares many features with hydrodynamic turbulence. For instance, in high Reynolds number flows, a large number of length scales are dynamically active and the nonlinear interactions are dominant in both the large-scale and the inertial-range dynamics. The dissipation is active mainly on the small scales of motion. There are also important differences with Navier–Stokes turbulence such as the number and the nature of the quadratic ideal invariants. In MHD the invariant quantities are the total energy, the magnetic helicity, and the cross helicity, whereas in fluids only energy is conserved. The description of the energy cascade from the largest scale of the turbulent system towards the small dissipative scales is usually done in terms of the energy flux through a given scale. Because of energy conservation, this flux is supposed to be constant in the inertial range. Using a Fourier representation for both the velocity and the magnetic fields, a finer description of the cascade can also be achieved by computing the energy transfers between subsets of modes with wave vectors that belong to a shell of the Fourier space.

Although the properties of energy fluxes in fluid turbulence have been studied in great details starting from Kolmogorov[1] (Lesieur[2] and references therein), this subject has not received much attention in MHD turbulence. Verma *et al.*,[3] and Dar, Verma, and Eswaran[4] computed energy fluxes in two-dimensional MHD turbulence using numerical simulations. Frick and Sokoloff[5] evaluated these fluxes using shell model. Analytically, the energy fluxes in MHD turbulence have been studied by Verma[6,7] using field-theoretic arguments, and by Goldreich and Sridhar[8] using kinetic theory. Shell-to-shell energy transfers have been computed in fluid turbulence by Zhou,[9] and Domaradzki and Rogallo[10] using eddy-damped quasinormal Markovian (EDQNM) calculation and numerical simulations. They reported the energy transfers to be mostly local. Pouquet, Frisch, and Léorat[11] have studied the energy transfers between various scales in MHD turbulence using EDQNM calculation. They reported nonlocal interactions and interpreted them as a consequence of a mean magnetic field (Alfvén effect) and of helicity. Dar, Verma, and Eswaran[4] numerically computed the shell-to-shell energy transfers for two-dimensional MHD turbulence. Recently, Verma and Ayyer[12] have computed the above quantities using a field-theoretic calculation.

The objective of this paper is to propose a detailed analysis of the nonlinear triad interactions in MHD turbulence and more specifically of shell-to-shell interactions. The concept of shell variables is naturally introduced when a Fourier decomposition of the fields is adopted. However, a real space version can be defined by considering the parts of the velocity and magnetic fields that correspond to structures with a given length scale. Since the conserved energy has two components in MHD, shell-to-shell interactions are expected to yield energy fluxes between the shells of velocity and magnetic fields. The definition of these shell-to-shell energy transfer rates and their links with the triad interactions in the MHD equations are presented in details in Sec. II. In particular, the shell-to-shell interactions are decomposed into forward (from large to small scales) and backward (from small to large scales) energy transfers. It is pointed out that such a decomposition is not unique and two possible strategies to identify the energy backscatter are suggested. They provide diagnostics that are expected to be relevant in the development of subgrid-scale models for large eddy simulations (LES).

In numerical simulations, only moderate Reynolds num-

bers have been achieved. In Sec. III, a simulation of isotropic decaying MHD turbulence using 512^3 Fourier modes is discussed. The energy fluxes as well as the shell-to-shell energy transfers between the velocity and the magnetic fields are computed from this simulation. They are presented in details in Sec. IV. A comparison with the theoretical estimates obtained by Verma and Ayyer[12] is also presented. Section V contains conclusion and a discussion on the possible importance of the present results in the modeling of MHD turbulence.

II. ENERGY TRANSFERS IN MHD TURBULENCE

A. Definitions

The equations for the incompressible MHD turbulence are

$$\frac{\partial \mathbf{u}}{\partial t} + (\mathbf{u}\cdot\boldsymbol{\nabla})\mathbf{u} = -\boldsymbol{\nabla} p + (\mathbf{b}\cdot\boldsymbol{\nabla})\mathbf{b} + \nu\boldsymbol{\nabla}^2\mathbf{u}, \tag{1}$$

$$\frac{\partial \mathbf{b}}{\partial t} + (\mathbf{u}\cdot\boldsymbol{\nabla})\mathbf{b} = (\mathbf{b}\cdot\boldsymbol{\nabla})\mathbf{u} + \eta\boldsymbol{\nabla}^2\mathbf{b}, \tag{2}$$

$$\boldsymbol{\nabla}\cdot\mathbf{u} = \boldsymbol{\nabla}\cdot\mathbf{b} = \mathbf{0}, \tag{3}$$

where ν and η are the fluid viscosity and the resistivity, respectively, and p is the total (thermal+magnetic) pressure field divided by the density, which has been taken to be a constant. The magnetic field has been represented in the Alfvén units and has the dimension of velocity. In incompressible flows, the pressure is supposed to adapt instantaneously to the velocity and magnetic field fluctuations in order to maintain the divergence-free condition. It is then the solution of the Poisson equation:

$$\nabla^2 p = -\partial_i\partial_j(u_i u_j - b_i b_j). \tag{4}$$

The primary objective of this section is to establish a formalism in which the energy transfer between structures of different sizes can be evaluated easily. The spectral representation of the fields are given by

$$\mathbf{u}(\mathbf{k}) = \int d\mathbf{x}\, \mathbf{u}(\mathbf{x}) e^{-i\mathbf{k}\cdot\mathbf{x}}, \tag{5}$$

$$\mathbf{b}(\mathbf{k}) = \int d\mathbf{x}\, \mathbf{b}(\mathbf{x}) e^{-i\mathbf{k}\cdot\mathbf{x}}. \tag{6}$$

For shell decomposition, the Fourier space is divided into shells s_n defined as the sets of wave vectors $\{\mathbf{k}\}$ such that $k_{n-1}=k_0 g^{n-1} \leqslant |\mathbf{k}| < k_n = k_0\, g^n$. In this definition, $g>0$ and $n \geqslant 1$, while k_0 is the smallest relevant wave number in the problem. The geometric growth of the shell boundaries is chosen because of the existence of power laws in the energy spectra. The shell decomposition for the velocity field is defined as follows:

$$\mathbf{u}^n(\mathbf{k}) = \begin{cases} \mathbf{u}(\mathbf{k}) & \text{if } \mathbf{k} \in s_n \\ 0 & \text{otherwise.} \end{cases} \tag{7}$$

The same decomposition will be used for the magnetic field.

The evaluation of shell-to-shell transfers may have some implications on the strategies adopted in turbulence modeling, especially in the framework of subgrid-scale modeling in large eddy simulation.[13,14] For this reason, it is also interesting to discuss the real space representation of the shell decomposition defined as

$$\mathbf{u}^n(\mathbf{x}) = \frac{1}{(2\pi)^3}\int d\mathbf{k}\, \mathbf{u}^n(\mathbf{k}) e^{+i\mathbf{k}\cdot\mathbf{x}}. \tag{8}$$

These definitions imply the following identities:

$$\mathbf{u}(\mathbf{x}) = \sum_n \mathbf{u}^n(\mathbf{x}), \quad \mathbf{b}(\mathbf{x}) = \sum_n \mathbf{b}^n(\mathbf{x}), \tag{9}$$

$$\mathbf{u}(\mathbf{k}) = \sum_n \mathbf{u}^n(\mathbf{k}), \quad \mathbf{b}(\mathbf{k}) = \sum_n \mathbf{b}^n(\mathbf{k}). \tag{10}$$

The total energy is the sum of the energy in each shell. Indeed,

$$E^u = \frac{1}{2}\sum_{\mathbf{k}} |\mathbf{u}(\mathbf{k})|^2 = \frac{1}{2}\sum_n \sum_{\mathbf{k}\in s_n} |\mathbf{u}(\mathbf{k})|^2 = \frac{1}{2}\sum_n \sum_{\mathbf{k}} |\mathbf{u}^n(\mathbf{k})|^2 = \sum_n E_n^u, \tag{11}$$

and using the Parseval's theorem the shell energy E_n^u is also given by

$$E_n^u = \frac{1}{2V}\int d\mathbf{x}\, \mathbf{u}^n(\mathbf{x})\cdot\mathbf{u}^n(\mathbf{x}). \tag{12}$$

The evolution equations for the shell energies in the ideal limit are given by

$$\dot{E}_n^u = \sum_m T_{n,m}^{u,u} + \sum_m T_{n,m}^{u,b}, \tag{13}$$

$$\dot{E}_n^b = \sum_m T_{n,m}^{b,u} + \sum_m T_{n,m}^{b,b}, \tag{14}$$

where $T_{n,m}^{Y,X}$ is the energy transfer from the field X in the shell s_m to the field Y in the shell s_n. The shell-to-shell transfers $T_{n,m}^{Y,X}$ give a more refined picture of the energy transfer processes than the energy fluxes through a given wave number. It is, however, worth computing these energy fluxes because they are one of the most important quantities in the inertial range. In MHD turbulence four types of energy fluxes are present. They are defined as

$$\Pi_{Y^>}^{X^<}(k_\ell) = \sum_{n\geqslant\ell}\sum_{m<\ell} T_{n,m}^{Y,X}. \tag{15}$$

These fluxes correspond to energy transfer from the inside of the wave number sphere (radius k_ℓ) of field X to the outside region of the same sphere of field Y. Furthermore, since kinetic and magnetic energies are not conserved separately, nontrivial fluxes of energy inside a wave vector domain can also be defined (for $X \neq Y$):

$$\Pi_{Y^<}^{X^<}(k_\ell) = \sum_{n<\ell}\sum_{m<\ell} T_{n,m}^{Y,X}, \tag{16}$$

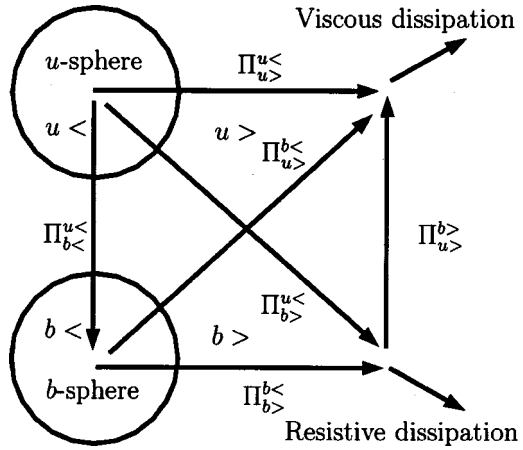

FIG. 1. Various energy fluxes in MHD turbulence. Π_Y^X represents energy flux from the inside of X sphere to the outside of Y sphere.

$$\Pi_{Y>}^{X>}(k_\ell) = \sum_{n\geqslant\ell}\sum_{m\geqslant\ell} T_{n,m}^{Y,X}. \tag{17}$$

The energy flux through the wave number sphere of radius k_ℓ is defined as

$$\begin{aligned}\Pi(k_\ell) &= \Pi_{u>}^{u<}(k_\ell) + \Pi_{u>}^{b<}(k_\ell) + \Pi_{b>}^{u<}(k_\ell) + \Pi_{b>}^{b<}(k_\ell)\\ &= \sum_{n\geqslant\ell}\sum_{m<\ell} (T_{n,m}^{u,u} + T_{n,m}^{u,b} + T_{n,m}^{b,u} + T_{n,m}^{b,b}).\end{aligned} \tag{18}$$

These various energy fluxes are illustrated in Fig. 1.

By definition, all the fluxes except $\Pi_{b<}^{u<}$ vanish at $k_\ell = k_{\max}$ (the maximum relevant wave number in the flow). $\Pi_{b<}^{u<}(k_{\max})$ is the total kinetic to magnetic energy transfer. Relations (15)–(17) show that the energy fluxes can be derived from the shell-to-shell energy transfer. Using the traditional terminology of subgrid-scale modeling, the energy fluxes characterize the transfer of energy from resolved to unresolved fields. The shell-to-shell energy transfers, however, characterize the transfer of energy between large-scale turbulent structures of size $1/k_n$ and small-scale turbulent structures of size $1/k_m$ assuming $k_n < k_m$. Some important properties of the shell-to-shell energy transfers are discussed in the following section.

B. Mode-to-mode transfers

Before discussing the shell-to-shell transfers, it is interesting to come back to some well-known properties of the mode-to-mode interactions. The formulas for mode-to-mode interactions are derived from the inviscid ($\nu=0$) and nonresistive ($\eta=0$) incompressible MHD equations in Fourier space given below,

$$\begin{aligned}\frac{\partial u_i(\mathbf{k})}{\partial t} &= -ik_i p(\mathbf{k}) - ik_j \sum_{\mathbf{k}=\mathbf{p}+\mathbf{q}} u_j(\mathbf{q})u_i(\mathbf{p})\\ &\quad + ik_j \sum_{\mathbf{k}=\mathbf{p}+\mathbf{q}} b_j(\mathbf{q})b_i(\mathbf{p}),\end{aligned} \tag{19}$$

$$\frac{\partial b_i(\mathbf{k})}{\partial t} = -ik_j \sum_{\mathbf{k}=\mathbf{p}+\mathbf{q}} u_j(\mathbf{q})b_i(\mathbf{p}) + ik_j \sum_{\mathbf{k}=\mathbf{p}+\mathbf{q}} b_j(\mathbf{q})u_i(\mathbf{p}). \tag{20}$$

Multiplying Eq. (19) by $u_i(-\mathbf{k})$ and Eq. (20) by $b_i(-\mathbf{k})$ and averaging the resulting equations yield

$$\begin{aligned}\left(\frac{\partial}{\partial t} + 2\nu k^2\right)\frac{1}{2}\langle|\mathbf{u}(\mathbf{k})|^2\rangle &= \sum_{\mathbf{k}+\mathbf{p}+\mathbf{q}=\mathbf{0}} \{-\mathrm{Im}\langle[\mathbf{k}\cdot\mathbf{u}(\mathbf{q})]\\ &\quad\times[\mathbf{u}(\mathbf{p})\cdot\mathbf{u}(\mathbf{k})]\rangle + \mathrm{Im}\langle[\mathbf{k}\cdot\mathbf{b}(\mathbf{q})]\\ &\quad\times[\mathbf{b}(\mathbf{p})\cdot\mathbf{u}(\mathbf{k})]\rangle\},\end{aligned} \tag{21}$$

$$\begin{aligned}\left(\frac{\partial}{\partial t} + 2\eta k^2\right)\frac{1}{2}\langle|\mathbf{b}(\mathbf{k})|^2\rangle &= \sum_{\mathbf{k}+\mathbf{p}+\mathbf{q}=\mathbf{0}} \{-\mathrm{Im}\langle[\mathbf{k}\cdot\mathbf{u}(\mathbf{q})]\\ &\quad\times[\mathbf{b}(\mathbf{p})\cdot\mathbf{b}(\mathbf{k})]\rangle + \mathrm{Im}\langle[\mathbf{k}\cdot\mathbf{b}(\mathbf{q})]\\ &\quad\times[\mathbf{u}(\mathbf{p})\cdot\mathbf{b}(\mathbf{k})]\rangle\},\end{aligned} \tag{22}$$

where Im stands for the imaginary part of the argument. Note that there is no contribution from the pressure field in Eq. (21). Indeed, in incompressible flows, the pressure force $\mathbf{k}p(\mathbf{k})$ is always perpendicular to the velocity field $-\mathbf{k}p(k)\cdot\mathbf{u}(\mathbf{k})=\mathbf{0}$. The pressure may however indirectly influence the evolution of the energy $\langle|\mathbf{u}(\mathbf{k})|^2\rangle$. Indeed, Eq. (21) is not closed and is only the first equation of a hierarchy which also contains dynamical equations for the higher-order moments of the velocity field. The pressure will appear in these higher order moment equations. We also stress that in compressible flows, the pressure force is not perpendicular to the velocity and it directly enters the equation for $\langle|\mathbf{u}(\mathbf{k})|^2\rangle$.

The energy transfer among the velocity modes has been studied by many authors.[2,4,15,16] In the present paper the energy fluxes and the shell-to-shell energy transfer rates are computed using the formalism of Dar, Verma, and Eswaran.[4] The details of this formalism is given in Dar, Verma, and Eswaran,[4] and Verma.[17] The four terms in the right-hand sides are called *mode-to-mode energy transfer rates* from u-to-u and b-to-u [in Eq. (21)], and b-to-b and u-to-b [in Eq. (22)]. They are represented by $S^{uu}(\mathbf{k}|\mathbf{p}|\mathbf{q})$, $S^{ub}(\mathbf{k}|\mathbf{p}|\mathbf{q})$, $S^{bb}(\mathbf{k}|\mathbf{p}|\mathbf{q})$, and $S^{bu}(\mathbf{k}|\mathbf{p}|\mathbf{q})$, respectively, i.e.,

$$S^{uu}(\mathbf{k}|\mathbf{p}|\mathbf{q}) = -\mathrm{Im}\{[\mathbf{k}\cdot\mathbf{u}(\mathbf{q})][\mathbf{u}(\mathbf{p})\cdot\mathbf{u}(\mathbf{k})]\}, \tag{23}$$

$$S^{ub}(\mathbf{k}|\mathbf{p}|\mathbf{q}) = \mathrm{Im}\{[\mathbf{k}\cdot\mathbf{b}(\mathbf{q})][\mathbf{b}(\mathbf{p})\cdot\mathbf{u}(\mathbf{k})]\}, \tag{24}$$

$$S^{bb}(\mathbf{k}|\mathbf{p}|\mathbf{q}) = -\mathrm{Im}\{[\mathbf{k}\cdot\mathbf{u}(\mathbf{q})][\mathbf{b}(\mathbf{p})\cdot\mathbf{b}(\mathbf{k})]\}, \tag{25}$$

$$S^{bu}(\mathbf{k}|\mathbf{p}|\mathbf{q}) = \mathrm{Im}\{[\mathbf{k}\cdot\mathbf{b}(\mathbf{q})][\mathbf{u}(\mathbf{p})\cdot\mathbf{b}(\mathbf{k})]\}. \tag{26}$$

By convention, $S^{YX}(\mathbf{k}|\mathbf{p}|\mathbf{q})$ represents the energy transfer from the mode $\mathbf{p}$ of field X (the second argument) to the mode $\mathbf{k}$ of field Y (the first argument). The mode $\mathbf{q}$ acts as a mediator. The functions $S^{YX}(\mathbf{k}|\mathbf{p}|\mathbf{q})$ have many interesting properties. For instance, the energy transfer rate from $\mathbf{X}(\mathbf{p})$ to $\mathbf{Y}(\mathbf{k})$ is the opposite of that from $\mathbf{Y}(\mathbf{k})$ to $\mathbf{X}(\mathbf{p})$, i.e.,

$$S^{YX}(\mathbf{k}|\mathbf{p}|\mathbf{q}) = -S^{XY}(\mathbf{p}|\mathbf{k}|\mathbf{q}). \tag{27}$$

Here X, Y stand for u or b fields.

In the presence of a mean magnetic field $\mathbf{B}_0$, the equations for both the velocity and the magnetic fields have ad-

ditional terms which read $-i\mathbf{B}_0\cdot\mathbf{k}\ \mathbf{b}(\mathbf{k})$ and $-i\mathbf{B}_0\cdot\mathbf{k}\ \mathbf{u}(\mathbf{k})$, respectively. These terms do not contribute to the global (kinetic+magnetic) energy equation. However, like the pressure force, they will indirectly affect the evolution of the energy through the higher order equations. This has to be expected since the presence of a mean magnetic field is known to have a strong influence on the dynamics of MHD turbulence.

In the following section we discuss shell-to-shell transfers in wave number space. We also construct formulas to measure forward energy transfer and backscatter in MHD turbulence.

C. Forward shell-to-shell energy transfer and backscatter

The shell-to-shell energy transfer rates can be expressed in terms of the mode-to-mode transfers as follows:

$$T_{n,m}^{Y,X}=\sum_{k\in S_n}\sum_{p\in S_m}S^{YX}(\mathbf{k}|\mathbf{p}|\mathbf{q}). \tag{28}$$

As a consequence of the symmetry property (27), the shell-to-shell transfer rates satisfy the relation

$$T_{n,m}^{Y,X}=-T_{m,n}^{X,Y}. \tag{29}$$

This has important consequences and in particular $\Pi_{b<}^{b<}(k_\ell)=\Pi_{u<}^{u<}(k_\ell)=0$ and $\Pi_{b>}^{b>}(k_\ell)=\Pi_{u>}^{u>}(k_\ell)=0$. Also, Eq. (29) implies that $T_{n,n}^{u,u}=T_{n,n}^{b,b}=0$. Note, however, that $T_{n,n}^{b,u}$ is not zero. A real space representation of the shell-to-shell transfers can easily be derived. As an example, the real space version of expression (28) for u-to-u energy transfer is given by

$$T_{n,m}^{u,u}=\int d\mathbf{x}\ u_i^n(\mathbf{x})\partial_j(u_i^m(\mathbf{x})u_j(\mathbf{x})). \tag{30}$$

Using integration by part, it is easy to show that it also satisfies the symmetry property $T_{n,m}^{u,u}=-T_{m,n}^{u,u}$.

In Kolmogorov's turbulence phenomenology, energy is transferred from small wave number shells to the large wave number shells, that is, $T_{nm}>0$ for $n>m$, and vice versa. Recent simulations however predict a certain amount of energy backscatter. In a mode-to-mode interaction, the definition of backscatter is unambiguous. Indeed, when k is smaller than p and $S^{YX}(\mathbf{k}|\mathbf{p}|\mathbf{q})<0$, it is natural to refer to this situation as energy backscatter (from the large wave vector $\mathbf{p}$ mode of variable X to the small wave vector $\mathbf{k}$ mode of variable Y). In a shell-to-shell description, the definitions of forward and backward energy transfers are not unique. One could of course consider that backscatter should correspond to $T_{n,m}^{X,Y}<0$; however, the shell-to-shell transfer contains a large number of mode-to-mode interactions that sometimes correspond to forward transfer and sometimes to energy backscatter. It is thus interesting to split $T_{n,m}^{X,Y}$ into forward and backward contributions. Such a separation is unavoidably quite arbitrary. Two possible representations are presented here.

In Fourier space, it would be tempting to define the forward and backward energy transfers from shell m to shell n $(m<n)$ as follows:

$$T_{n,m,(k)}^{Y,X,(+)}=\sum_{k\in s_n}\left[\sum_{p\in s_m}S^{YX}(\mathbf{k}|\mathbf{p}|\mathbf{q})\right]_+ \tag{31}$$

and

$$T_{n,m,(k)}^{Y,X,(+)}=\sum_{k\in s_n}\left[\sum_{p\in s_m}S^{YX}(\mathbf{k}|\mathbf{p}|\mathbf{q})\right]_-, \tag{32}$$

where the operators $[\cdots]_+$ and $[\cdots]_-$ are defined by

$$[x]_+=\begin{cases}x & \text{if } x>0\\ 0 & \text{if } x\leqslant 0,\end{cases}\qquad [x]_-=\begin{cases}0 & \text{if } x>0\\ x & \text{if } x\leqslant 0.\end{cases} \tag{33}$$

In the above definitions, the additional superscript $+$ or $-$ corresponds to forward transfer and backscatter of energy. The additional subscript k is required since these definitions are not necessarily the same in Fourier space and in real space, as it will be shown below. Unfortunately,

$$T_{n,m,(k)}^{Y,X,(+)}\neq -T_{m,n,(k)}^{X,Y,(-)}. \tag{34}$$

We expect that $T_{n,m,(k)}^{Y,X,(+)}$ and $T_{m,n,(k)}^{X,Y,(-)}$ must be equal and opposite. This problem is solved by introducing the following definitions for the forward and backward energy transfers:

$$T_{n,m,(k)}^{Y,X,(+)}=\frac{1}{2}\left(\sum_{k\in s_n}\left[\sum_{p\in s_m}S^{YX}(\mathbf{k}|\mathbf{p}|\mathbf{q})\right]_+ -\sum_{p\in s_m}\left[\sum_{k\in s_n}S^{YX}(\mathbf{k}|\mathbf{p}|\mathbf{q})\right]_-\right), \tag{35}$$

$$T_{n,m,(k)}^{Y,X,(-)}=\frac{1}{2}\left(\sum_{k\in s_n}\left[\sum_{p\in s_m}S^{YX}(\mathbf{k}|\mathbf{p}|\mathbf{q})\right]_- -\sum_{p\in s_m}\left[\sum_{k\in s_n}S^{YX}(\mathbf{k}|\mathbf{p}|\mathbf{q})\right]_+\right). \tag{36}$$

With these definitions, the amount of backscatter from shell n to shell m is indeed equal to the amount of forward transfer from shell m to shell n.

The above definitions are intrinsically based on the Fourier representation of velocity and magnetic fields. It is interesting to provide equivalent diagnostics based on the real space version of the fields. Obviously, it is also desirable to impose the same symmetry condition for the real space representation of forward and backward energy transfers:

$$T_{n,m,(x)}^{Y,X,(+)}=-T_{m,n,(x)}^{X,Y,(-)}. \tag{37}$$

Such a property is easily imposed when the following definitions are adopted:

$$T_{n,m}^{u,u}=\frac{1}{2}\int d\mathbf{x}[u_i^n(\mathbf{x})\partial_j(u_i^m(\mathbf{x})u_j(\mathbf{x})) -u_i^m(\mathbf{x})\partial_j(u_i^n(\mathbf{x})u_j(\mathbf{x}))]. \tag{38}$$

Obviously, integration by part shows that the definitions (30) and (38) are equivalent. Moreover, expression (38) allows us to define shell-to-shell forward and backward transfers as

$$T_{n,m,(x)}^{u,u,(+)}=\frac{1}{2}\int d\mathbf{x}[u_i^n(\mathbf{x})\partial_j(u_i^m(\mathbf{x})u_j(\mathbf{x})) -u_i^m(\mathbf{x})\partial_j(u_i^n(\mathbf{x})u_j(\mathbf{x}))]_+, \tag{39}$$

$$T^{u,u,(-)}_{n,m,(x)} = \frac{1}{2}\int d\mathbf{x}[u_i^n(\mathbf{x})\partial_j(u_i^m(\mathbf{x})u_j(\mathbf{x})) - u_i^m(\mathbf{x})\partial_j(u_i^n(\mathbf{x})u_j(\mathbf{x}))]_-, \quad (40)$$

which satisfy the property given by Eq. (37).

It is important to note, however, that in general $T^{u,u,(+)}_{n,m,(x)} \neq T^{u,u,(+)}_{n,m,(k)}$. This shows that the definition of shell-to-shell backscatter is not unique and, as will be shown in the following section, the properties of $T^{u,u,(+)}_{n,m,(x)}$ and $T^{u,u,(+)}_{n,m,(k)}$ appear to be quite different.

In the next two sections we will describe the numerical method and results regarding the shell-to-shell energy transfer rates and fluxes for decaying three-dimensional MHD turbulence.

III. SIMULATION DETAILS

The numerical simulation used for evaluating the shell-to-shell transfers has been done using a fully-dealiased pseudospectral code on a 512^3 grid. The initial energy spectrum for both the velocity and the magnetic fields were generated with the function

$$E(k) = \frac{ak^4}{(k^4+q^4)^{1+\alpha}}\exp(-bk^\beta), \quad (41)$$

with $a=10.6$, $q=1.5$, $b=0.02$, $\alpha=1.233$, and $\beta=1.1$. It was done in order to match the spectra measured in the Comte-Bellot–Corrsin[18] experiment at stage 1. The initial phases were randomly generated. Physically acceptable phases were built up using an initialization procedure during which the flow is evolved according to the MHD equations but rescaled at each time step to match the experimental spectrum. This procedure was applied until the skewness of the velocity derivative reached a quasiconstant value of −0.26. The resulting fields are considered as the initial conditions for the MHD turbulence simulation.

The Reynolds number R_λ (based on Taylor's microscale) for the initial field was 159. The initial values of global variables are $E^u=E^b=31.2$. The cross helicity as well as the magnetic helicity, though not exactly zero, can be considered as negligible in the simulation. The geometry is a $(2\pi)^3$ box, and both viscosity and resistivity were set to 3×10^{-3}. A third-order Runge–Kutta scheme is used to integrate the MHD equations. The time step dt was computed automatically using the Courant–Friedrichs–Lewy criterion, and it was of the order of 2×10^{-3}. The simulation was evolved up to nondimensional time $t^*=t/t_{\text{eddy}}=1.74$, where

$$t_{\text{eddy}} = E_0/\varepsilon_0, \quad (42)$$

E_0 and ε_0 being, respectively, the total energy and dissipation rate at $t^*=0$. Figure 2 shows the decay of kinetic, magnetic, and total energies and the evolution of Alfvén ratio $r_A=E^u/E^b$. The Alfvén ratio decreases along with energy and approaches 0.41 at the final time. Note that in many computer simulations and solar wind[19] measurements the Alfvén ratio decreases and saturates around 0.5.

The normalized cross helicity increases very slowly from near 0 to ≈0.1, and it can be ignored in our analysis.

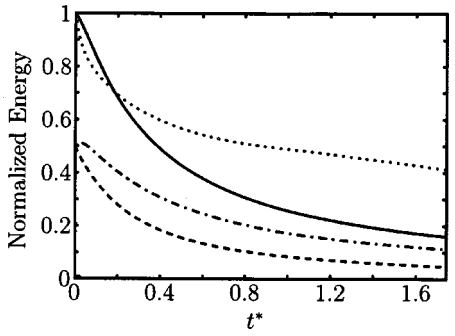

FIG. 2. Temporal evolution of the normalized total energy (—), magnetic energy (-·-·-), kinetic energy (----), and Alfvèn ratio (···).

The increase in the normalized cross helicity has been seen in earlier numerical simulations. This phenomena, called "dynamic alignment," has been discussed by Matthaeus and Montgomery,[20] and others. In addition, the magnetic and kinetic helicities are negligible in the simulation.

The direct numerical simulation (DNS) described in the preceding section is performed using a pseudospectral code. Both the shell-to-shell transfer rates in real space $T^{u,u,(\pm)}_{n,m,(x)}$ and in Fourier space $T^{u,u,(\pm)}_{n,m,(k)}$ have been computed quite easily from the DNS code by following the procedure described by Domaradzki and Rogallo,[10] and Dar, Verma, and Eswaran.[4] The computation of these quantities, however, requires an intensive postprocessing and the results presented in the following are limited to a single frame corresponding to $t^*=1.74$. At this time, a significant fraction of the total initial energy has been dissipated and the initial condition is not expected to influence the profiles of shell-to-shell energy transfer. Figure 3 illustrates the compensated kinetic, magnetic, and total energy spectra $E(k)k^{5/3}$ at $t^*=1.74$. As previously observed by Müller and Biskamp,[21] the total energy spectra in the inertial range are fitted reasonably well by a power law for $k\approx(10-25)$. The inertial range is quite narrow. However, this narrow range is very useful for deriving some important properties of self-similar shell-to-shell interactions. The energy spectra at other times are similar.

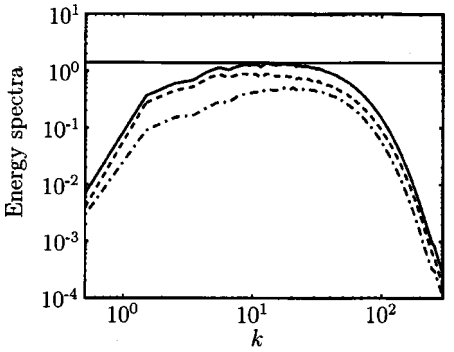

FIG. 3. Compensated spectra $E(k)k^{5/3}$ of total energy (—), magnetic energy (----), and kinetic energy (-·-·-) at $t^*=1.74$.

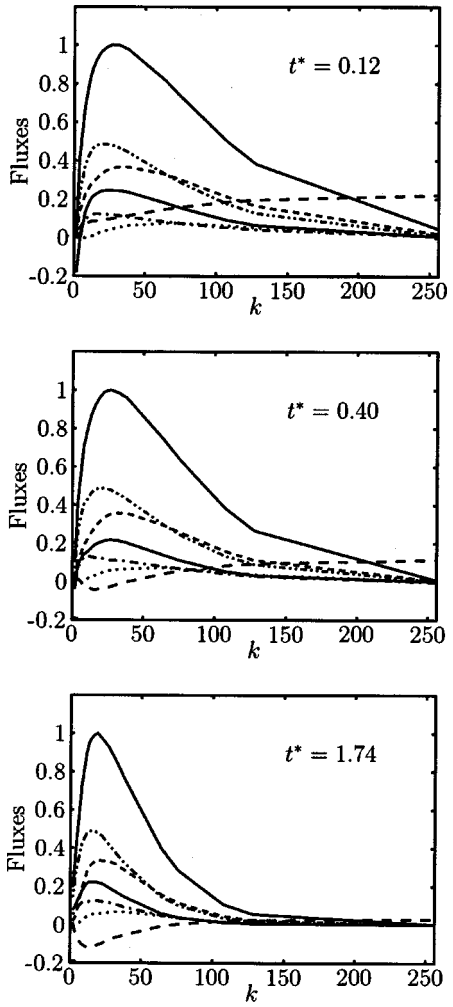

FIG. 4. Energy fluxes vs k: $\pi_{\rm tot}$ (—), $\pi^{u<}_{u>}$ ($\cdots\cdots$), $\pi^{b<}_{b>}$ (----), $\pi^{u<}_{b>}$ ($\cdots\cdot$), $\pi^{b<}_{u>}$ ($\cdot\cdot\cdot$), $\pi^{u<}_{b<}$ (---), and $\pi^{b>}_{u>}$ (—). Top—$t^*=0.12$, $r_A=0.75$; middle—$t^*=0.40$, $r_A=0.63$; bottom—$t^*=1.73$, $r_A=0.41$.

IV. NUMERICAL RESULTS

A. Energy fluxes

The energy fluxes defined by the relation (15) can be derived from the shell-to-shell energy transfers. It is, however, interesting to analyze these fluxes first since they provide a global picture of the various energy exchanges that influence the MHD turbulence. The energy fluxes depend on the wave number as well as on time. These dependencies are illustrated on Fig. 4 in which the wave number dependency is shown at three different times in the energy decay.

A small range of wave numbers near $k=10-25$ where the energy fluxes are somewhat flat is identified as the inertial range. This is approximately the same range found in the analysis of the energy spectra. Within this range, the fluxes are almost wave number independent and it is convenient to introduce the following nondimensional quantities,

$$\pi^X_Y = \frac{\Pi^X_Y(k \in \text{inertial range})}{\Pi}, \tag{43}$$

where $\Pi=\Pi^{u<}_{u>}+\Pi^{u<}_{b>}+\Pi^{b<}_{u>}+\Pi^{b<}_{b>}$ is the total flux in the inertial range. The values of these quantities are shown in Table I.

TABLE I. The numerical (sim) and theoretical (th) values of energy fluxes in MHD turbulence for $r_A=0.75$, 0.6, and 0.41. The theoretical values have been computed by Verma (Ref. 7) using field-theoretic techniques.

π/r_A	0.75 (sim)	0.75 (th)	0.6 (sim)	0.6 (th)	0.4 (sim)	0.4 (th)
$\pi^{u<}_{u>}$	0.075	0.078	0.073	0.024	0.066	0.024
$\pi^{u<}_{b>}$	0.49	0.38	0.49	0.31	0.49	0.31
$\pi^{b<}_{u>}$	0.12	0.20	0.13	0.40	0.13	0.40
$\pi^{b<}_{b>}$	0.37	0.34	0.36	0.27	0.34	0.27
$\pi^{u<}_{b>}$	0.22	⋯	−0.024	⋯	−0.12	⋯
$\pi^{u>}_{b>}$	0.24	⋯	0.22	⋯	0.22	⋯
K^+	2.8	1.53	3.02	1.51	3.0	1.51
K^u	1.1	0.65	1.2	1.50	1.1	1.50
ν^*	⋯	1.3	⋯	3.07	⋯	3.07
η^*	⋯	0.63	⋯	0.40	⋯	0.40

Figure 5 shows the evolution of the normalized inertial-range fluxes. Interestingly, all the normalized inertial-range fluxes except $\pi^{u<}_{b<}$ are approximately time independent. Time is however not the most relevant parameter and it is conveniently replaced by the Alfvén ratio. The quantity $\pi^{u<}_{b<}$ decreases from 0.22 at r_A near 1 to ≈ -0.12 near $r_A=0.4$ and is reasonably well fitted by a linear relation:

$$\pi^{u<}_{b<} \approx \gamma_1(r_A - r^*_A). \tag{44}$$

This result indicates that for $r_A > r^*_A \approx 0.63$, large-scale kinetic energy is transferred to large-scale magnetic energy. The direction of transfer is reversed for $r_A < r^*_A$ (more magnetically dominated regime). The best fit gives $\gamma_1=0.56$. Further studies are definitively required to determine whether the values of γ_1 and r^*_A are universal or dependent on the initial condition.

The fluxes $\Pi^{u<}_{u>}$, $\Pi^{u<}_{b>}$, $\Pi^{b<}_{u>}$, and $\Pi^{b<}_{b>}$ are forward, that is, from small to large wave numbers. Also, $\Pi^{b>}_{u>}>0$. The net transfer from kinetic energy to magnetic energy is defined by

$$\Pi^u_b = \Pi^{u<}_{b<} + \Pi^{u<}_{b>} + \Pi^{u>}_{b<} + \Pi^{u>}_{b>}. \tag{45}$$

It is easy to check that $\Pi^u_b=\Pi^{u<}_{b<}(k_{\rm max})$. The kinetic-to-magnetic energy transfer takes place until r_A reaches around $r_A=\overline{r_A}\approx 0.37$. The best fit is $\pi^u_b=\gamma_2(r_A-\overline{r_A})$ where $\gamma_2\approx 0.57$. For $r_A=\overline{r_A}$ and beyond, the net energy transfer from kinetic to magnetic is almost zero. Again the universal character of

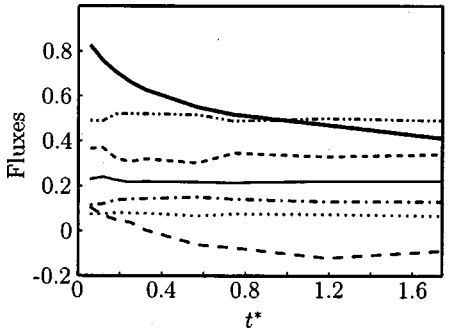

FIG. 5. Energy fluxes in the inertial range vs time. The fluxes shown are $\pi^{u<}_{u>}$ ($\cdots\cdots$), $\pi^{b<}_{b>}$ (----), $\pi^{u<}_{b>}$ ($\cdots\cdot$), $\pi^{b<}_{u>}$ ($\cdot\cdot\cdot$), $\pi^{u<}_{b<}$ (---), and $\pi^{b>}_{u>}$ (—). The thick (—) line represents the Alfvén ratio.

the number $\overline{r_A}$ and γ_2 definitively requires further investigations. Note that at $r_A=0.63$, $\Pi_{b<}^{u<}(k_{\max})>0$ (see Fig. 4), hence a net kinetic-to-magnetic energy transfer is taking place even when $\Pi_{b<}^{u<}\approx 0$ for $r_A=0.63$.

The value of $\pi_{u>}^{u<}$ is quite small, hence the *u*-to-*u* transfer seems to be dominated by the *u*-to-*b* transfer in MHD turbulence, at least when $r_A<1$. In Table I, the numerical values of normalized energy fluxes are compared with Verma's theoretical predictions[7] calculated using field-theoretic method. It is however important to stress that Verma's theoretical predictions are based on several assumptions, e.g., steady state and Kolmogorov's spectra in the inertial range that are not satisfied in the numerical simulation. In addition, Verma's theoretical calculations cannot predict $\pi_{b<}^{u<}$ and $\pi_{b>}^{u>}$. Comparison of numerical and theoretical values, however, shows a reasonably good agreement. The differences in the values are the largest for $\pi_{b>}^{u<}$ and $\pi_{u>}^{b<}$, which may be due to nonlocal interactions as discussed below.

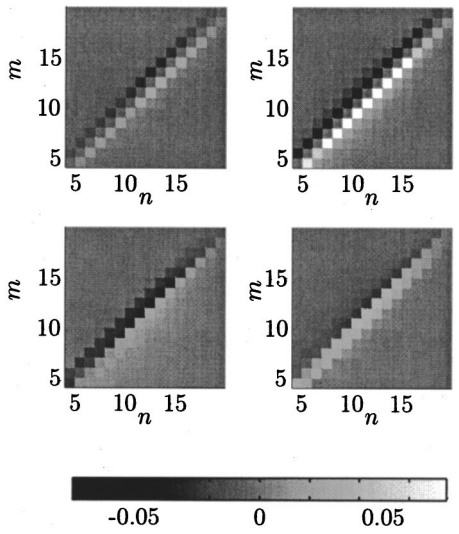

FIG. 6. Values of $T_{n,m}^{u,u}/\Pi$ (upper left), $T_{n,m}^{b,b}/\Pi$ (upper right), $T_{n,m}^{b,u}/\Pi$ (lower left), and $T_{n,m}^{u,b}/\Pi$ (lower right) at time $t^*=1.74$.

B. Shell-to-shell energy transfer

The data analyzed in the following sections have been produced by a spectral code with 512^3 modes in a cubic geometry. The largest complete shell (i.e., excluding corner modes) is thus bounded by $k=256$. Both the velocity and the magnetic fields have been decomposed according to the methodology presented in Sec. II A. The ratio between the upper and the lower bound of the shell boundaries has been chosen small enough ($g=2^{1/4}$) to ensure a fairly refined analysis of the shell interactions. However, the first shells corresponding to the lowest wave vectors must be wider. Otherwise, the first shells contain only few modes and their statistical analysis becomes meaningless. In the data postprocessing, the first three shells have thus been chosen to be $s_1\equiv\{\mathbf{k}\}$ such that $0<k\leqslant 2$, $s_2\equiv\{\mathbf{k}\}$ such that $2<k\leqslant 4$, and $s_3\equiv\{\mathbf{k}\}$ such that $4<k\leqslant 8$. Also, in order to limit the number of shells, the last shell (which entirely lies in the dissipation range) is also wider $s_{20}\equiv\{\mathbf{k}\}$ such that $128<k\leqslant 256$. Between $k=8$ and $k=128$, the wave number space is split into shell s_n bounded by k_n and k_{n+1} where $k_n=2^{(n+8)/4}$.

Since we are primarily interested in the self-similar properties of the shell-to-shell energy transfers, the following discussion will be limited to the shells that are defined using self-similar bounds, i.e., s_4-s_{19}. The four normalized shell-to-shell energy transfers $T_{nm}^{Y,X}/\Pi$ are computed using the method described in Sec. II C. The shell-to-shell transfers are conveniently represented using two-dimensional density plot corresponding to a matrix of energy transfers. For instance the total (forward+backscatter) transfers are represented in Fig. 6.

As expected, these transfers are dominated by the diagonal contributions that correspond to local shell-to-shell transfers, i.e., transfers between neighbor shells. All the values of the shell-to-shell transfers appear to be negligible for $|n-m|>4$, which correspond to interaction between the shells characterized by wave vectors with amplitude ratios of 2 or larger. All the four transfers correspond to direct (forward) cascades of energy. Indeed, the shell-to-shell transfers are systematically positive when $n>m$ and systematically negative when $n<m$. Finally, the dominant shell-to-shell exchanges clearly appear to be in the *b*-to-*b* interactions. For the same shell, $T_{n,n}^{u,u}$ and $T_{n,n}^{b,b}$ vanish, but $T_{n,n}^{u,b}$ is positive and $T_{n,n}^{b,u}$ is negative.

It is interesting also to investigate the same graphs for the purely forward contributions [the backscatter contribution are directly obtained from the same graphs using the imposed symmetry property (34) between forward and backscatter energy transfers]. For instance, Fig. 7 shows that the purely forward transfer is also very much local. However, Fig. 7 reveals that the quantity $T_{n,m,(k)}^{u,b,(+)}/\Pi$ has the largest amplitude, so that the dominant forward shell-to-shell exchange of energy is between *u* and *b*. It is also interesting to notice that, in order to obtain the best contrast, the scales are not the same in Figs. 6 and 7. Indeed, the forward transfers are by definition always positive and the scale has been adapted accordingly. However, the amplitude of the forward transfer

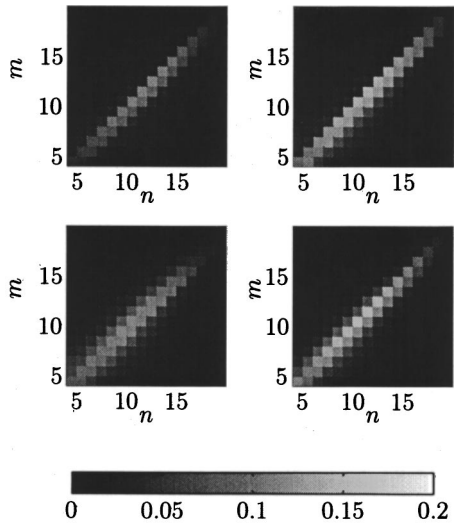

FIG. 7. Values of $T_{n,m,(k)}^{u,u,(+)}/\Pi$ (upper left), $T_{n,m,(k)}^{b,b,(+)}/\Pi$ (upper right), $T_{n,m,(k)}^{b,u,(+)}/\Pi$ (lower left), and $T_{n,m,(k)}^{u,b,(+)}/\Pi$ (lower right) at time $t^*=1.74$.

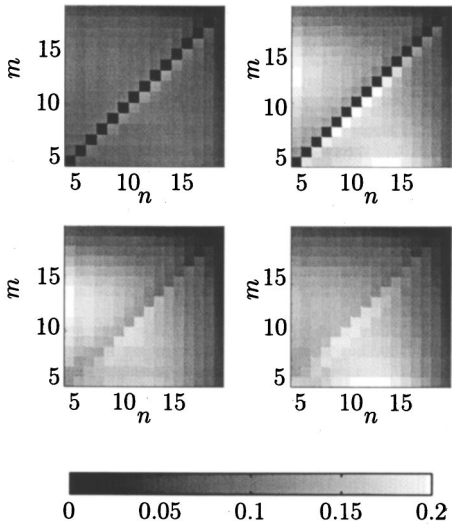

FIG. 8. Values of $T^{u,u,(+)}_{n,m,(x)}/\Pi$ (upper left), $T^{b,b,(+)}_{n,m,(x)}/\Pi$ (upper right), $T^{b,u,(+)}_{n,m,(x)}/\Pi$ (lower left), and $T^{u,b,(+)}_{n,m,(x)}/\Pi$ (lower right) at time $t^*=1.74$.

is significantly larger than that of the total transfer, meaning that the total transfer contains two important parts corresponding to forward and backward transfers that largely cancel each other.

The picture is drastically different if we consider the real space definition of backscatter. Figure 8 shows now that the purely forward transfer defined using formulas (39) and (40) is much more nonlocal. A local forward transfer is still present and is characterized by the diagonal contribution. However, large values of the forward energy transfer defined in real space are observed for $n-m$ as large as 10.

C. Inertial-range analysis

As already mentioned, the existence of an inertial range is questionable in the simulation presented here. However, both the spectra and the flux analysis tend to show the appearance of a narrow range of wave vectors between $k\approx 10$ and $k\approx 25$ with properties compatible with an inertial range. Hence, shells s_5-s_{10} will be considered to belong to the inertial range. Within this range the energy transfers are anticipated to be self-similar, i.e., the transfer from shell 6 to shell 8 should be the same as the transfer from shell 7 to shell 9. This is indeed observed in Fig. 9, in which the normalized energy transfers $T^{Y,X}_{nm}/\Pi$ versus $n-m$ are plotted for various m's in the inertial range $(5\leqslant n,m\leqslant 10)$. These figures also confirm that the inertial-range shell-to-shell energy transfers are always from small to large wave numbers (forward transfer). Indeed, they are positive for $n>m$ and negative for $n<m$. The dominant u-to-u and b-to-b transfers are to the neighbor shell $n-m=1$ and decreases quite rapidly, confirming that these energy transfers are fairly local. On the contrary, the dominant u-to-b transfer is to the same wave number shell $n=m$ and decays more slowly.

The same graphs are presented in Figs. 10 and 11 for the forward transfers in wave and real spaces. The energy backscatter is readily deduced from these graphs using the symmetry property (34). Again, these quantities appear to be

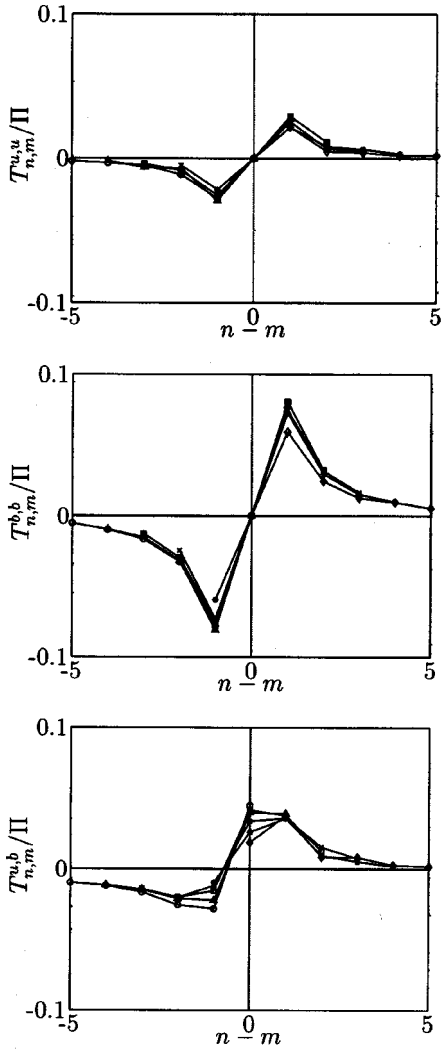

FIG. 9. Plots of T^{uu}_{nm}/Π (top), T^{bb}_{nm}/Π (middle), and T^{ub}_{nm}/Π (bottom) normalized shell-to-shell energy transfers vs $n-m$ for n and m in the range [5,10], $\diamond$, $m=5$; $*$, $m=6$; $\times$, $m=7$; $\square$, $m=8$; $\triangle$, $m=9$; $\bigcirc$,$m=10$.

self-similar. It is interesting to notice the important difference between $T^{X,Y,(+)}_{n,m,(x)}$ and $T^{X,Y,(+)}_{n,m,(k)}$. By definition, $T^{u,u,(+)}_{n,m,(x)}$ and $T^{b,b,(+)}_{n,m,(x)}$ vanish for $n=m$. Also, they do not rapidly go to zero for increasing $n-m$. On the contrary, $T^{u,u,(+)}_{n,m,(k)}$ and $T^{b,b,(+)}_{n,m,(k)}$ reach a maximum for $n=m$ and decay fairly rapidly for large $n-m$. These properties confirm the previous remark that the forward transfers expressed by $T^{X,Y,(+)}_{n,m,(k)}$ are very much local while those expressed by $T^{X,Y,(+)}_{n,m,(x)}$ are much more nonlocal.

These results show that the choice of the definition of backscatter may quite strongly influence the interpretation of the diagnostics. This might be seen as an undesirable property. Moreover, in the framework of LES, the arbitrariness appearing in the definition of backscatter could be considered as a reason to discard this diagnostics in the assessment of subgrid-scale model. This is not the point of view advocated here. Indeed, when the definition of backscatter has been clearly and cleanly given, there is no ambiguity on how to compute the forward and backward energy transfers. These transfers can then be used as valid guides in the de-

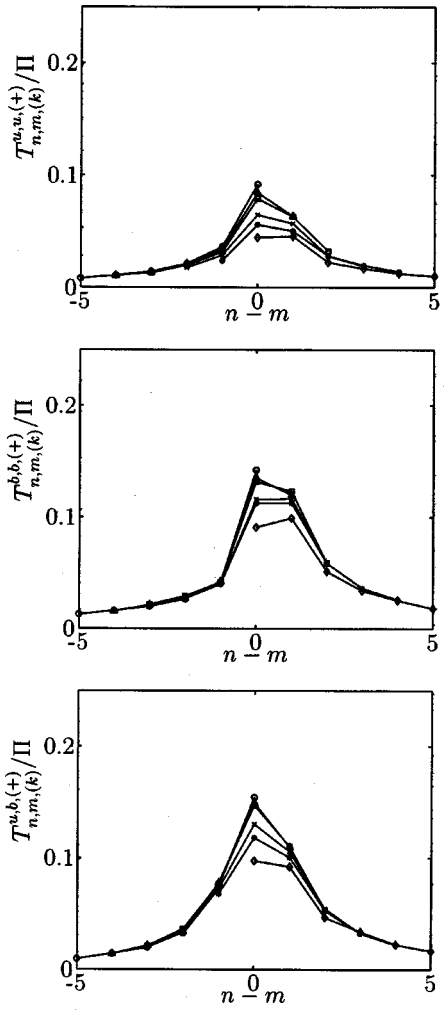

FIG. 10. Plots of $T^{u,u,(+)}_{nm,(k)}/\Pi$ (top), $T^{b,b,(+)}_{nm,(k)}/\Pi$ (middle), and $T^{u,b,(+)}_{nm,(k)}/\Pi$ (bottom) normalized shell-to-shell energy transfers vs $n-m$ for n and m in the range [5,10], $\diamond$, $m=5$; $*$, $m=6$; $\times$, $m=7$; $\square$, $m=8$; $\triangle$, $m=9$; $\bigcirc$, $m=10$.

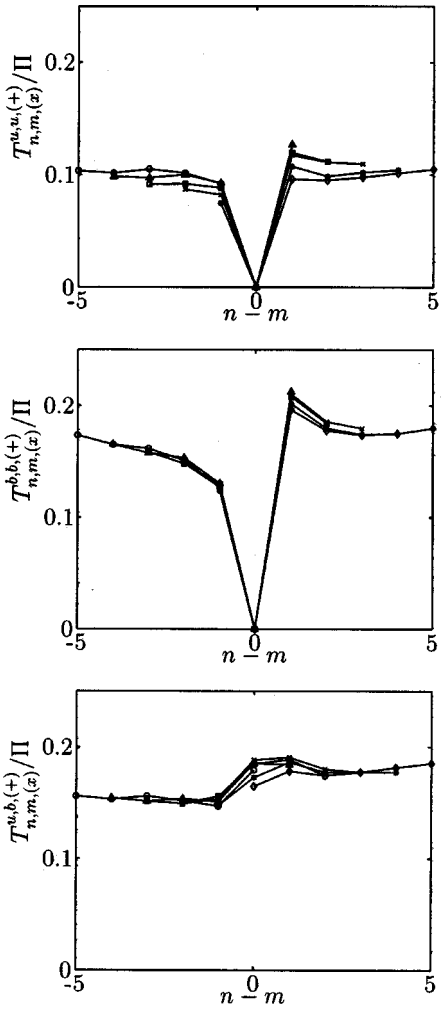

FIG. 11. Plots of $T^{u,u,(+)}_{nm,(x)}/\Pi$ (top), $T^{b,b,(+)}_{nm,(x)}/\Pi$ (middle), and $T^{u,b,(+)}_{nm,(x)}/\Pi$ (bottom) normalized shell-to-shell energy transfers vs $n-m$ for n and m in the range [5,10], $\diamond$, $m=5$; $*$, $m=6$; $\times$, $m=7$; $\square$, $m=8$; $\triangle$, $m=9$; $\bigcirc$, $m=10$.

velopment of subgrid-scale models that are supposed to reproduce the energy transfers between resolved and unresolved scales as accurately as possible.

V. DISCUSSION

The energy transfer rates between different shells of wave vectors have been analyzed in details for turbulent velocity and magnetic fields by solving the incompressible MHD equations. This analysis is based on a decomposition of the fields into modes with characteristic wavelengths corresponding to increasingly fine scales. The boundaries of these shells follow a power law, anticipating a self-similar properties of the shell-to-shell energy exchanges.

In incompressible MHD turbulence four energy exchanges can be identified between two wave number shells. These energy transfers are *u-u*, *u-b*, *b-u*, and *b-b*. This is in contrast with Navier–Stokes turbulence in which only one independent flux can be defined. Except for this difference, the methodology for defining the shell-to-shell transfers is very much inspired by earlier works on hydrodynamic turbulence.

The results presented in Sec. IV show that, as usually anticipated in the analysis of mode interactions in turbulence, the total (backscatter+forward) energy transfers are very much local. The wave number shells that are characterized by wave vectors with an amplitude ratio of 2 or more do not exchange significant amount of energy. The result is less obvious if the forward transfer of energy and the backscatter are studied separately. First, it is shown that the definition of backscatter is not unique and two possible definitions are proposed. The pictures obtained with these two representations are fairly different. In the Fourier representation, the forward and the backward transfers, like the total energy exchanges, are quite local. On the contrary, the real space decomposition shows very nonlocal exchanges of energy between the shells.

The knowledge of the detailed backscatter and forward energy transfers is an interesting guide to describe the physics of the nonlinear interactions in turbulence. It is also a valuable diagnostics in the framework of subgrid-scale modeling. Indeed, LES have become more and more popular as a tool to investigate high Reynolds number flows in

hydrodynamics.[22] In LES, large and small scales of motion are artificially separated using a local averaging procedure usually considered to be a filtering operator. The resulting locally averaged equations for the large scales are solved numerically. They contain however unknown terms representing the influence of the smallest scales (subgrid-scale terms). Such a strategy allows for significant savings in computer times as well as in memory requirements. Traditionally, the subgrid-scale models are assessed using two methods. In *a priori* techniques, the model is compared with the real subgrid-scale terms that are obtained when filtering a large-scale database obtained by solving directly the Navier–Stokes equation for a very simple geometry (usually for isotropic turbulence or for the channel flow). In *a posteriori* techniques, the LES equations with a model for the unknown subgrid-scale terms are solved and their results are compared to direct numerical simulations or experimental results. These *a posteriori* techniques are much more costly, especially in MHD where detailed experimental data are difficult to collect. It is thus important to have *a priori* tests that are as refined as possible. The detailed knowledge of the shell-to-shell energy transfers definitively provides such a refined *a priori* assessment.

Finally, we point out a reasonable agreement between the shell-to-shell energy transfers determined here from a numerical simulation of decaying MHD turbulence and the theoretical predictions of Verma and Ayyer[12] who computed shell-to-shell energy transfers using field-theoretic method. Despite significant differences between the assumptions required to perform the theoretical computation and the actual conditions of the numerical simulation, most of the characteristics of the total energy transfers are well reproduced by the theory.

ACKNOWLEDGMENTS

This work was supported in part by the Communauté Française de Belgique (Grant No. ARC02/07-283) and by the contract of association EURATOM—Belgian state. The content of the publication is the sole responsibility of the authors and it does not necessarily represent the views of the Commission or its services. One of the authors, M.K.V., acknowledges the kind hospitality provided by the hosts during his visit to ULB where this work was done. D.C. and O.D. are supported by the Fonds National pour la Recherche Scientifique (Belgium).

[1] A. Kolmogorov, Dokl. Akad. Nauk SSSR **30**, 299 (1941).
[2] M. Lesieur, *Turbulence in Fluids—Stochastic and Numerical Modelling* (Kluwer Academic, Dordrecht, 1990).
[3] M. K. Verma, M. Goldstein, S. Ghosh, and W. Stribling, J. Geophys. Res. **101**, 21619 (1996).
[4] G. Dar, M. K. Verma, and V. Eswaran, Physica D **157**, 207 (2001).
[5] P. Frick and D. Sokoloff, Phys. Rev. E **57**, 4155 (1998).
[6] M. K. Verma, Phys. Rev. E **64**, 026305 (2001).
[7] M. K. Verma, Pramana **61**, 577 (2003).
[8] P. Goldreich and P. Sridhar, Astrophys. J. **438**, 763 (1995).
[9] Y. Zhou, Phys. Fluids A **5**, 1092 (1993).
[10] J. Domaradzki and R. Rogallo, Phys. Fluids A **2**, 413 (1990).
[11] A. Pouquet, U. Frisch, and J. Léorat, J. Fluid Mech. **77**, 321 (1976).
[12] M. K. Verma and A. Ayyer, "Energy transfer and locality in magnetohydrodynamic turbulence," J. Fluid Mech. (to be published).
[13] O. Agullo, W.-C. Müller, B. Knaepen, and D. Carati, Phys. Plasmas **8**, 3502 (2001).
[14] W.-C. Müller and D. Carati, Comput. Phys. Commun. **147**, 544 (2002).
[15] R. Kraichnan, J. Fluid Mech. **47**, 525 (1971).
[16] M. Stanišić, *The Mathematical Theory of Turbulence* (Springer, Berlin, 1988).
[17] M. K. Verma, Phys. Rep. **401**, 232 (2004).
[18] G. Comte-Bellot and S. Corrsin, J. Fluid Mech. **48**, 273 (1971).
[19] W. Matthaeus and L. Goldstein, J. Geophys. Res. **87**, 6011 (1982).
[20] W. Matthaeus and D. Montgomery, in *Statistical Physics and Chaos in Fusion Plasmas*, edited by C. Horton and L. Reichl (Wiley, New York, 1984), p. 285.
[21] W.-C. Müller and D. Biskamp, Phys. Rev. Lett. **84**, 475 (2000).
[22] R. Rogallo and P. Moin, Annu. Rev. Fluid Mech. **16**, 99 (1984).